# PROCEEDINGS OF SPIE

SPIEDigitalLibrary.org/conference-proceedings-of-spie

# Volumetric microfabrication of helical structures for industrial applications

He Cheng, Pooria Golvari, Chun Xia, Mingman Sun, Meng Zhang, et al.

He Cheng, Pooria Golvari, Chun Xia, Mingman Sun, Meng Zhang, Stephen M. Kuebler, Xiaoming Yu, "Volumetric microfabrication of helical structures for industrial applications," Proc. SPIE 12054, Novel Patterning Technologies 2022, 1205409 (25 May 2022); doi: 10.1117/12.2614703



Event: SPIE Advanced Lithography + Patterning, 2022, San Jose, California, United States

# Volumetric microfabrication of helical structures for industrial applications

He Cheng<sup>a</sup>, Pooria Golvari<sup>b</sup>, Chun Xia<sup>a</sup>, Mingman Sun<sup>c</sup>, Meng Zhang<sup>c</sup>, Stephen M. Kuebler<sup>abd</sup>, Xiaoming Yu\*<sup>a</sup>

aCREOL, The College of Optics and Photonics, University of Central Florida, Orlando, Florida 32816, USA;
bDepartment of Chemistry, University of Central Florida, Orlando, Florida 32816, USA;
cDepartment of Industrial and Manufacturing Systems Engineering, Kansas State University, Manhattan, Kansas 66506, USA;
dDepartment of Material Science and Engineering, University of Central Florida, Orlando, Florida, 32816, USA

#### **ABSTRACT**

Helical structures with novel optical and mechanical properties have been demonstrated and are commonly used in different fields such as metamaterials, microfluidics and cell scaffold. None of conventional fabrication methods has the throughput or flexibility required for patterning large surface area with tunable pitch. In this paper, we report a novel method for high-throughput volumetric fabricating helical structures with tunable shape based on multiphoton polymerization (MPP) using single-exposure, self-accelerating beam with adjustable rotating intensity profile. The light-fields are generated based on high-order Bessel modes and an analytical model is derived to describe the generation and propagation of light-fields. The method is used to fabricated micro-helices with different pitches and handedness in SU-8 photoresist. Beam splitting and galvo-scanning can be implemented in the system. The fabrication of large-scale helical matrices is demonstrated. Compared to point-by-point scanning, our method increases the fabrication throughput by orders of magnitude, paving the way for adopting MPP for mass production of functional devices in many industrial applications. **Keywords:** Multiphoton polymerization; spatial beam shaping; volumetric microfabrication; self-accelerating beam.

#### 1. INTRODUCTION

Recently, helical microstructures have drawn increased attention because they exhibit novel optical and mechanical properties in various fields. Many prototype optical devices utilizing helical microstructures have been demonstrated, such as broadband circular polarizers [1,2], circular polarization converters [3], and wave plates [4]. Helical microchannels are used as microfluidic mixers [5,6]. Driven by the magnetic field, magnetic micro-helices can be used as micro-robots for cargo transportation [7,8]. Helical microstructures could also have useful applications as microfluidic sensors [9], heat diffusers [10,11], and scaffolds for growing cells [12].

Fabrication of helical structures often requires nonplanar fabrication methods such as multiphoton polymerization (MPP). MPP is a direct laser writing technique that is increasingly used [2,3,13–18] because it offers a means for creating almost arbitrarily complex three-dimensional (3D) structures with high precision. However, MPP is time-consuming due to the point-by-point writing strategy. It often requires hours or even days to fabricate a single part depending on the size and resolution. The slow fabrication speed of conventional MPP is the key factor that limits its wider application for industrial manufacturing. One approach for increasing fabrication speed is to turn the point-by-point scanning into a volumetric process by spatially shaping the laser beam so that one entire layer or even the complete structure could be fabricated with a single exposure. Layer-by-layer fabrication of various extruded tube-like 3D structures has been demonstrated by focusing shaped Bessel beam [19–23]. The fabrication is achieved by scanning the focused beam along the optical axis, but the increase in throughput is limited because axial scanning is still needed. Volumetric fabrication with single exposure has also been demonstrated, including the fabrication of high-aspect-ratio structures using Bessel-[24,25] and axilens beams [26]. However, the shape of the structures is limited by the needle-like focal shape and thus lacks variety. Vortex beams have been used to fabricate 3D helical structures with limited aspect ratios [27–29]. For good optical and mechanical functionality, helical structures often need to have multiple pitches and high aspect-ratios, e.g., to be effective as microfluidic mixers [5,6] or metamaterials [1,2,14,30,31]. However, methods reported in Refs. [27–29]

Novel Patterning Technologies 2022, edited by Eric M. Panning, J. Alexander Liddle, Proc. of SPIE Vol. 12054, 1205409 · © 2022 SPIE · 0277-786X · doi: 10.1117/12.2614703

only achieved low aspect-ratio helical structure with less than one complete rotation. So far, no method has the throughput required for fabricating over a large area with tall helices that have multiple variable pitches.

In this work, we describe a volumetric fabrication approach based on MPP with single-exposure using a new class of self-accelerating beams (SABs) with rotating intensity distribution. A complete account of the theory and derivation is reported elsewhere [32]. The proposed SABs are based on the superposition of two high-order Bessel beam modes. Compared to existing SABs with constant rotation rate [33–36], the proposed beams feature tunable angular acceleration (variable pitch), which means the rotation rate (and hence pitch) can be tailored to follow a nearly arbitrary profile within the limit of optical arrangement, while other SABs with angular acceleration reported in Refs. [37–39] follow a specific equation with single tuning parameter. We have developed an analytical model to describe the generation and propagation of the SABs in free space and between media. Closed-form solutions for the intensity distribution and rotation rate are derived, thus a direct calculation of computer-generated hologram (CGH) for the SABs can be performed. The analytic model makes it easier to synthesize 3D beams and is an improvement on the iterative algorithms used by others. Microhelices with constant and varying pitches are fabricated with a single exposure in the forms of individual helices and matrices of helices. With optimization, this method can be used to increase throughput by more than two orders of magnitude over conventional MPP and paves the way for mass microfabrication of helical structures for many industrial applications, including metamaterials, microfluidics and biomaterials.

### 2. THEORY AND DESIGN OF COMPUTER-GENERATED HOLOGRAMS

We apply CGH on a phase-only SLM to generate the SABs. The foundation of our SABs is the superposition of two high-order Bessel beam modes. The Bessel-beam phase (BBP) of two Bessel beam modes with orders l and m can be expressed in terms of a common axicon phase component  $k_{\perp}r$  and their individual azimuthal phase components  $l\theta$  and  $m\theta$  [40–43]:

$$BBP_l = -k_{\perp}r + l\theta, \qquad BBP_m = -k_{\perp}r + m\theta. \tag{1}$$

Inspired by the concept of geometrical r-z mapping relationship of zero-order Bessel beam [44], we introduce a rotation-tuning function v(r) to modulate the phase along the radial direction. This extra phase term, which we call "radial phase modulation" (RPM), is written as:

$$RPM_l = -RPM_m = -\frac{l-m}{2}v(r)r. \tag{2}$$

The superposition of these two components gives a transmittance function  $T(r,\theta) = \exp(-i(BBP_l + RPM_l)) + \exp(-i(BBP_m + RPM_m))$  which is the desired CGH. As  $T(r,\theta)$  has both phase and amplitude information, in order to display it on the phase-only SLM, we use a phase encoding method that is based on a pair of complementary "binary amplitude masks" (BAMs) with checkerboard patterns [45]. After encoding, the phase becomes:

$$\varphi(r,\theta) = (BBP_l + RPM_l) \times BAM_l + (BBP_m + RPM_m) \times BAM_m. \tag{3}$$

The encoded phase  $\varphi(r,\theta)$  is displayed on the SLM as it is illuminated with a Gaussian beam. The beam reflected off SLM is sent into a 4-f system with a low-pass filter applied at the Fourier plane. Using Fresnel diffraction theory and the stationary phase method [40,46,47], we derive a closed-form solution for the intensity distribution at point  $(r, \theta, z)$  after image plane [32]. The expression of the intensity distribution can be separated into a product of two terms. The first term describes the intensity variation along the z-axis, which has an extended depth of field similar to a zero-order Gaussian-Bessel beam. The second term describe an intensity distribution that is rotating along z-axis. The rotation rate can be expressed as:

$$\omega(z) \equiv \frac{d\theta}{dz} = -\frac{k_{\perp}}{k} M^2 v' \left( M^2 \frac{k_{\perp}}{k} z \right) z - \frac{k_{\perp}}{k} M^2 v \left( M^2 \frac{k_{\perp}}{k} z \right), \tag{5}$$

where v' represents the first derivative of v with respect to z. Equation (5) establishes a "forward" relationship between the rotation rate  $\omega(z)$  and rotation tunning function v(r). Treating v(r) as unknown, we can rewrite Equation (5) as an ordinary linear differential equation which has the following general solution:

$$v(r) = \frac{1}{r} \int -M^{-2} \frac{k}{k_{\perp}} \omega \left( M^{-2} \frac{k}{k_{\perp}} r \right) dr. \tag{6}$$

Equation (6) provides a "reverse" relationship between  $\omega(z)$  and v(r) and is the key to generating SABs in this work. This equation can be solved analytically or numerically to obtain a CGH that produces a beam with a specific rotation

profile described by  $\omega(z)$ . The SAB's rotation can be engineered directly without having to employ phase-retrieval algorithms [48]. Using a similar method, the propagation of the proposed SABs through the planer interface can also be derived. It is found that refraction from the interface does not affect the transverse intensity distribution of the SABs; only the rotation rate decreases when the light propagates through a medium with higher refractive index.

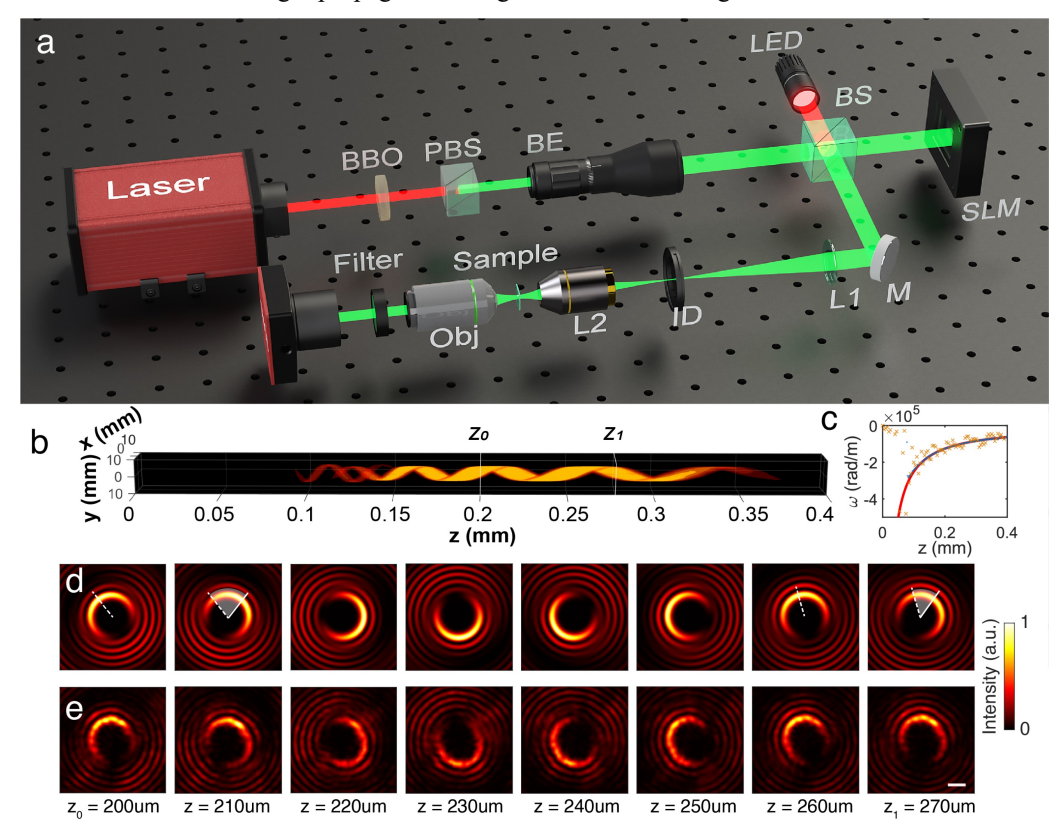


Figure 1. Generation of helical structures using self-accelerating beams (SABs). (a) Experimental setup: BBO, beta barium borate crystal; PBS, polarizing beam splitter; BE, beam expander; BS, non-polarizing beam splitter; SLM, spatial light modulator; M, mirror; L, lens; ID, iris diaphragm; Obj, objective lens; CMOS, complementary metal-oxide-semiconductor. (b-e) Comparison of simulated and measured SAB with decelerated rotation rate in free space. Phase order l=-10 and m=-9. (b) Iso-intensity contours of a simulated SAB in air. The threshold intensity (normalized) is set to 0.5. (d) Simulated and (e) measured x-y intensity distribution. Scale bar represents 5  $\mu$ m. (c) Rotation rate  $\omega$  along optical axis. Red curves, designed profile; orange points, measured data.

### 3. EXPERIMENTAL RESULTS

In the experiment setup as shown in Figure 1a, the light-source is a femtosecond laser (Pharos, Light Conversion) that generates pulses having a temporal full-width at half-maximum (FWHM) of 170 fs, center wavelength of  $\lambda_0 = 1030$  nm, and repetition rate of 100 kHz. The output beam is frequency-doubled by a beta barium borate (BBO) crystal, expanded and collimated, and sent to a spatial light modulator (SLM), which is a reflecting, phase-only, liquid-crystal-on-silicon device (Meadowlark Optics,  $1920 \times 1150$  pixels, 256 gray levels, 9.2 µm pixel-pitch). CGHs generated with the proposed method are displayed on the SLM. The beam is reflected off the SLM and directed into a 4-f system composed of a planoconvex lens (f = 750 mm) and an objective lens ( $10 \times$ , NA = 0.3, focal length = 18 mm) and then spatially filtered by an iris placed at the Fourier plane of the 4-f system. The optical field at the focal plane of the objective lens is a demagnified replica of that formed on the SLM. The SABs generated by the proposed method are measured in free space to validate the theory. A CMOS camera with a  $20 \times$  objective lens shown in Figure 1 is mounted on a motorized stage to image a series of transverse (x-y) intensity distributions at positions z along the optical axis (Figure 1d).

The SABs are first generated in space using proposed method and compared with simulation results. One example of SAB is shown in Figure 1b-e, which has a decreasing rotation rate  $\omega = -25.13z^{-1}$  rad/m in air and topological charges l = -10, m = -9 and  $k_{\perp} = 6.6 \times 10^4$  m<sup>-1</sup>. Part of the experimental measurements of the transverse intensity profile

along the optical axis are shown in Figure 1d to show the good agreement with the simulation results using scalar diffraction theory (Figure 1c). The SAB has a "C" shape transverse intensity profile with a radius of ~5  $\mu$ m. The SAB shows a long depth of focus, greater than 300  $\mu$ m. In space, the intensity distribution of the SAB has a helical shape that resembles a twisted strap (Figure 1b). We measured the rotation by extracting the directional angle  $\alpha$  from x-y intensity profile of SAB and calculating the rotation rate by  $\omega(z) = \Delta \alpha/\Delta z$ . The white sector shapes in Figure 1d show that  $\Delta \alpha$  has reduced from z = 210 mm to z = 270 mm. As shown in Figure 1c, the rotation rate matches the theory. The deviation is due to the aforementioned distortions in experimentally generated beam profiles. We also observe a deviation from the "C" shape in x-y plane intensity distribution both experimentally and in simulation at the beginning of the SAB where the rotation rate exceeds  $2 \times 10^5$  rad/m. This is shown in Figure 1b on the left of the SAB. Here the beam appears as a "double helix" and indicates the limit of the highest rotation rate that can be obtained with this method. By using Equation (6), we are able to obtain SABs with different rotation rates along the optical axis as will be demonstrated in the fabrication results.

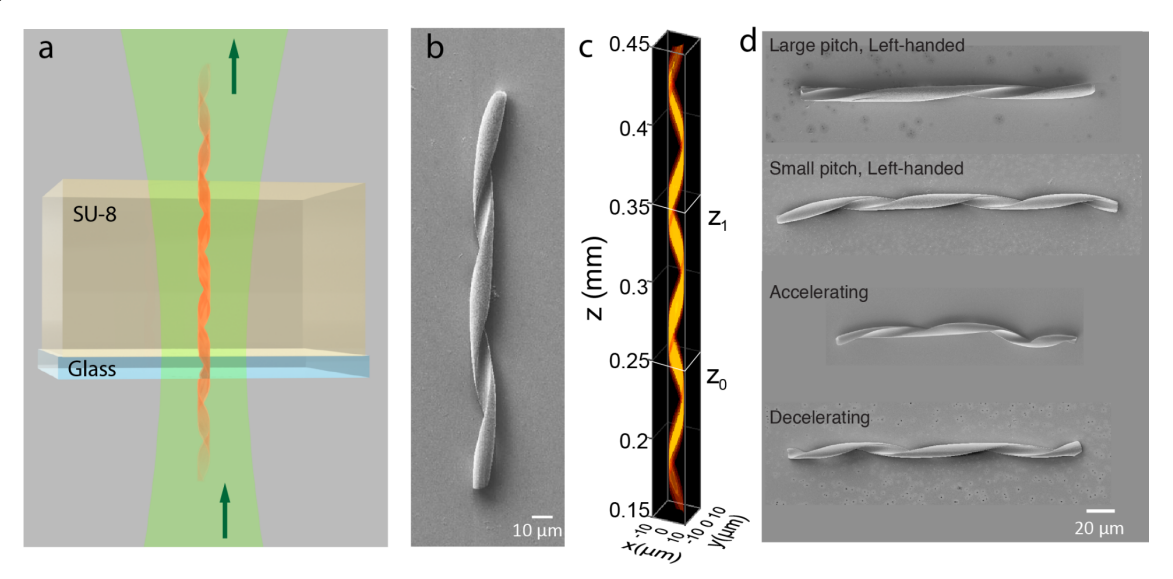


Figure 2. Volumetric fabrication of micro-helix with a single exposure of SAB. (a) Illustration of exposure in the SU-8 sample. The green arrow shows the beam propagation direction. (b) SEM images of a fabricated single helix. (c) Simulation of the SAB used in fabrication in (b). (d) Examples of single helices with different rotations.

Equation (6) was used to design CGHs that generate SABs for fabricating helices in SU-8 2075 (Kayaku Advanced Materials). SU-8 is a negative photoresist commonly used in fabrication high-aspect-ratio functional devices with MPP [49]. The CGHs have phase order (l, m) = (-10, -9) and  $k_{\perp} = 6.6 \times 10^4$  m<sup>-1</sup>. The demagnified beam is directed into a layer of SU-8 that was spin-coated on a glass substrate (Figure 2a) and baked prior to exposure to remove the solvent [1]. Each helix was patterned with static exposure (no scanning) and an exposure time of less than 0.15 ms. After exposure, the sample is baked to activate cross-linking and developed in propylene glycol methyl ether acetate (PGMEA) to remove unexposed material [1,2]. The resulting structures were imaged by scanning electron microscopy (SEM). The results are shown in Figure 2b. Fresnel diffraction theory is used to simulate the SABs in photoresist. An example of an iso-intensity contour of the simulated SABs used in fabrication is plotted in Figure 2c together with cross-sections of the intensity distribution. The SAB demonstrated here features a constant rotation rate along the optical axis. Figure 2b and 3c show a comparison between the simulated beam shape and the fabricated micro-helices. The length of the helix is limited by the thickness of the spin-coated SU-8 layer. Because of the high aspect-ratio, a single helix does not withstand the capillary force during development and is found lying down on the glass substrate. By tunning the rotation of SAB using Equation (6) we could fabricate helices with different pitch sizes and handedness as shown in Figure 2d.

By performing a series of single exposures with lateral sample translation(Figure 3a), helical matrices can be fabricated. Figure 3 shows several matrices, each consisting of  $30 \times 30$  helices with a certain pitch and handedness. The fabrication time for each matrix is approximately 15 min. Since each individual helix is fabricated volumetrically, most of the time is spent on translating the sample. In terms of fabrication volume per unit time, the method reported here is more than 100 times faster than point-by-point scanning for similar structures reported in [13]. The fabrication time could be further reduced by adding a galvanometer scanner to increase the speed of lateral scanning. The helical structures shown in Figure

3 can be used as metamaterials at terahertz frequencies [50,51]. Further reduction in pitch can be achieved by tighter focusing (which may require the use of vectorial diffraction theories) and will enable application at optical frequencies.

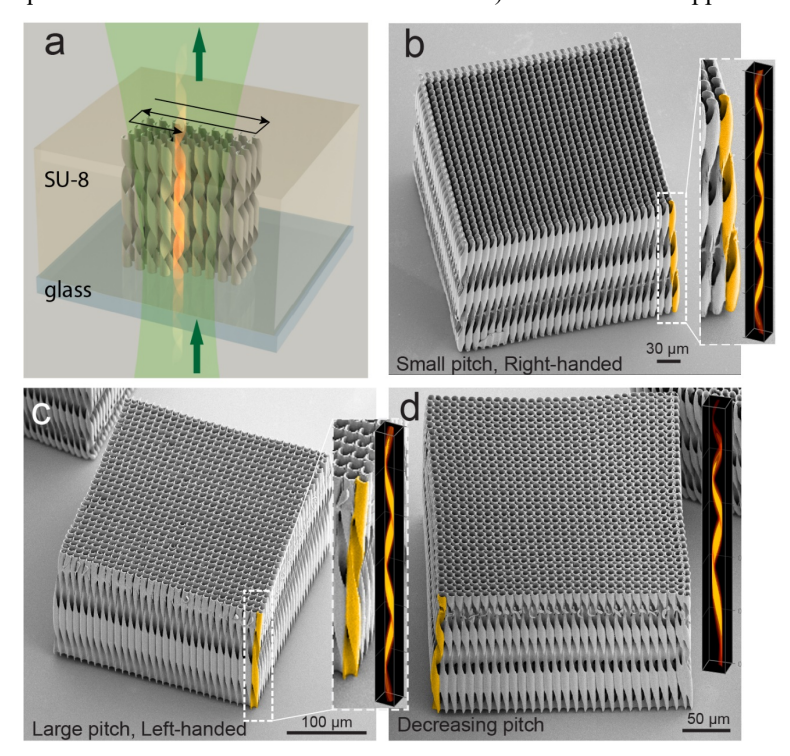


Figure 3. Matrices of various helical structures fabricated by a combination of exposure and lateral sample translation.

## 4. CONCLUSION

We have demonstrated a method for volumetric microfabrication of helical structures with a tunable axial pitch by proposing a new class of SABs and adapting them to MPP. The SABs are based on the superposition of high-order Bessel modes and form non-diffracting transverse intensity profiles that rotate along the optical axis. A closed-form expression was derived that can be used to directly synthesize targeted CGH and SAB without resorting to iterative algorithms. SABs can be generated with independently adjustable transverse width and rotational pitch. Single micro-helices can be fabricated volumetrically with a single exposure of SAB. Matrices of helices with various pitch and handedness were fabricated rapidly in SU-8 with good agreement with the beam shapes. The approach reduced fabrication time by two orders of magnitude relative to conventional point-by-point scanning MPP. As a first step toward full volumetric fabrication, our method addresses the low throughput issue of MPP and represents a leap forward towards mass microfabrication in industrial applications.

## Acknowledgement

This material is based partly upon work supported by the National Science Foundation under Grants No. 1711356 and 1846671.

#### REFERENCES

- 1. J. K. Gansel, M. Thiel, M. S. Rill, M. Decker, K. Bade, V. Saile, G. von Freymann, S. Linden, and M. Wegener, "Gold Helix Photonic Metamaterial as Broadband Circular Polarizer," Science **325**(5947), 1513–1515 (2009).
- 2. J. K. Gansel, M. Latzel, A. Frölich, J. Kaschke, M. Thiel, and M. Wegener, "Tapered gold-helix metamaterials as improved circular polarizers," Appl. Phys. Lett. **100**(10), 101109 (2012).
- 3. J. Kaschke, L. Blume, L. Wu, M. Thiel, K. Bade, Z. Yang, and M. Wegener, "A Helical Metamaterial for

- Broadband Circular Polarization Conversion," Adv. Opt. Mater. 3(10), 1411–1417 (2015).
- 4. C. Wu, H. Li, X. Yu, F. Li, H. Chen, and C. T. Chan, "Metallic Helix Array as a Broadband Wave Plate," Phys. Rev. Lett. **107**(17), 177401 (2011).
- 5. M. K. S. Verma, S. R. Ganneboyina, Rakshith, and A. Ghatak, "Three-Dimensional Multihelical Microfluidic Mixers for Rapid Mixing of Liquids," Langmuir **24**(5), 2248–2251 (2008).
- 6. C. Shan, F. Chen, Q. Yang, Z. Jiang, and X. Hou, "3D Multi-Microchannel Helical Mixer Fabricated by Femtosecond Laser inside Fused Silica," Micromachines 9(1), 29 (2018).
- 7. S. Tottori, L. Zhang, F. Qiu, K. K. Krawczyk, A. Franco-Obregon, and B. J. Nelson, "Magnetic helical micromachines: Fabrication, controlled swimming, and cargo transport," Adv. Mater. **24**(6), 811–816 (2012).
- 8. L. Zhang, J. J. Abbott, L. Dong, B. E. Kratochvil, D. Bell, and B. J. Nelson, "Artificial bacterial flagella: Fabrication and magnetic control," Appl. Phys. Lett. **94**(6), 3–5 (2009).
- 9. W. Li, G. Huang, J. Wang, Y. Yu, X. Wu, X. Cui, and Y. Mei, "Superelastic metal microsprings as fluidic sensors and actuators," Lab Chip **12**(13), 2322 (2012).
- 10. M. I. Hussain, G. H. Lee, and B. Engineering, "Numerical thermal analysis of helical-shaped heat exchanger to improve thermal stratification inside solar," Proc. Int. Conf. Agric. Eng. Zurich 6(10), 6–10 (2014).
- 11. E. S. Shukri, "Numerical Comparison of Temperature Distribution in an Annular Diffuser Fitted with Helical Screw-Tape Hub and Pimpled Hub," Energy Procedia **141**, 625–629 (2017).
- 12. A. V. Do, B. Khorsand, S. M. Geary, and A. K. Salem, "3D Printing of Scaffolds for Tissue Regeneration Applications," Adv. Healthc. Mater. 4(12), 1742–1762 (2015).
- 13. M. Thiel, M. Decker, M. Deubel, M. Wegener, S. Linden, and G. von Freymann, "Polarization Stop Bands in Chiral Polymeric Three-Dimensional Photonic Crystals," Adv. Mater. 19(2), 207–210 (2007).
- M. Thiel, M. S. Rill, G. von Freymann, and M. Wegener, "Three-Dimensional Bi-Chiral Photonic Crystals," Adv. Mater. 21(46), 4680–4682 (2009).
- 15. J. Kaschke and M. Wegener, "Gold triple-helix mid-infrared metamaterial by STED-inspired laser lithography," Opt. Lett. **40**(17), 3986 (2015).
- 16. Y. Liu, J. Campbell, O. Stein, L. Jiang, J. Hund, and Y. Lu, "Deformation Behavior of Foam Laser Targets Fabricated by Two-Photon Polymerization," Nanomaterials **8**(7), 498 (2018).
- 17. G. Kumi, C. O. Yanez, K. D. Belfield, and J. T. Fourkas, "High-speed multiphoton absorption polymerization: Fabrication of microfluidic channels with arbitrary cross-sections and high aspect ratios," Lab Chip **10**(8), 1057–1060 (2010).
- 18. S. Kawata, H. B. Sun, T. Tanaka, and K. Takada, "Finer features for functional microdevices," Nature **412**(6848), 697–698 (2001).
- 19. L. Yang, S. Ji, K. Xie, W. Du, B. Liu, Y. Hu, J. Li, G. Zhao, D. Wu, W. Huang, S. Liu, H. Jiang, and J. Chu, "High efficiency fabrication of complex microtube arrays by scanning focused femtosecond laser Bessel beam for trapping/releasing biological cells," Opt. Express 25(7), 8144 (2017).
- 20. S. Ji, L. Yang, C. Zhang, Z. Cai, Y. Hu, J. Li, D. Wu, and J. Chu, "High-aspect-ratio microtubes with variable diameter and uniform wall thickness by compressing Bessel hologram phase depth," Opt. Lett. **43**(15), 3514 (2018).
- 21. S. Ji, L. Yang, Y. Hu, J. Ni, W. Du, J. Li, G. Zhao, D. Wu, and J. Chu, "Dimension-Controllable Microtube Arrays by Dynamic Holographic Processing as 3D Yeast Culture Scaffolds for Asymmetrical Growth Regulation," Small 13(34), 1701190 (2017).
- 22. L. Yang, D. Qian, C. Xin, Z. Hu, S. Ji, D. Wu, Y. Hu, J. Li, W. Huang, and J. Chu, "Two-photon polymerization of microstructures by a non-diffraction multifoci pattern generated from a superposed Bessel beam," Opt. Lett. 42(4), 743 (2017).
- 23. L. Yang, D. Qian, C. Xin, Z. Hu, S. Ji, D. Wu, Y. Hu, J. Li, W. Huang, and J. Chu, "Direct laser writing of complex microtubes using femtosecond vortex beams," Appl. Phys. Lett. **110**(22), 221103 (2017).
- 24. H. Cheng, C. Xia, M. Zhang, S. M. Kuebler, and X. Yu, "Fabrication of high-aspect-ratio structures using Bessel-beam-activated photopolymerization," Appl. Opt. **58**(13), D91 (2019).
- 25. J. Jezek, T. Cizmár, V. Nedela, and P. Zemánek, "Formation of long and thin polymer fiber using nondiffracting beam.," Opt. Express **14**(19), 8506–8515 (2006).
- 26. D. Pan, B. Xu, S. Liu, J. Li, Y. Hu, D. Wu, and J. Chu, "Amplitude-phase optimized long depth of focus femtosecond axilens beam for single-exposure fabrication of high-aspect-ratio microstructures," Opt. Lett. **45**(9), 2584 (2020).
- 27. S.-J. Zhang, Y. Li, Z.-P. Liu, J.-L. Ren, Y.-F. Xiao, H. Yang, and Q. Gong, "Two-photon polymerization of a

- three dimensional structure using beams with orbital angular momentum," Appl. Phys. Lett. **105**(6), 061101 (2014).
- 28. J. Ni, C. Wang, C. Zhang, Y. Hu, L. Yang, Z. Lao, B. Xu, J. Li, D. Wu, and J. Chu, "Three-dimensional chiral microstructures fabricated by structured optical vortices in isotropic material," Light Sci. Appl. 6(7), e17011–e17011 (2017).
- Y. Li, L. Liu, D. Yang, Q. Zhang, H. Yang, and Q. Gong, "Femtosecond laser nano/microfabrication via three-dimensional focal field engineering," in *Laser-Based Micro- and Nanoprocessing XI* (2017), 10092(May), p. 100920B.
- 30. J. Kaschke, J. K. Gansel, and M. Wegener, "On metamaterial circular polarizers based on metal N-helices," Opt. Express **20**(23), 26012 (2012).
- 31. J. K. Gansel, M. Wegener, S. Burger, and S. Linden, "Gold helix photonic metamaterials: A numerical parameter study," Opt. Express **18**(2), 1059 (2010).
- 32. H. Cheng, P. Golvari, C. Xia, M. Sun, M. Zhang, S. M. Kuebler, and X. Yu, "High-throughput microfabrication of axially tunable helices," Photonics Res. **10**(2), 303 (2022).
- 33. C. Vetter, T. Eichelkraut, M. Ornigotti, and A. Szameit, "Optimization and control of two-component radially self-accelerating beams," Appl. Phys. Lett. **107**(21), 211104 (2015).
- 34. R. Rop, A. Dudley, C. López-Mariscal, and A. Forbes, "Measuring the rotation rates of superpositions of higher-order Bessel beams," J. Mod. Opt. **59**(3), 259–267 (2012).
- 35. C. Vetter, T. Eichelkraut, M. Ornigotti, and A. Szameit, "Generalized Radially Self-Accelerating Helicon Beams," Phys. Rev. Lett. **113**(18), 183901 (2014).
- 36. R. Vasilyeu, A. Dudley, N. Khilo, and A. Forbes, "Generating superpositions of higher–order Bessel beams," Opt. Express 17(26), 23389 (2009).
- 37. C. Schulze, F. S. Roux, A. Dudley, R. Rop, M. Duparré, and A. Forbes, "Accelerated rotation with orbital angular momentum modes," Phys. Rev. A **91**(4), 043821 (2015).
- 38. C. Vetter, A. Dudley, A. Szameit, and A. Forbes, "Real and virtual propagation dynamics of angular accelerating white light beams," Opt. Express **25**(17), 20530 (2017).
- 39. J. Webster, C. Rosales-Guzmán, and A. Forbes, "Radially dependent angular acceleration of twisted light," Opt. Lett. **42**(4), 675 (2017).
- 40. A. Vasara, J. Turunen, and A. T. Friberg, "Realization of general nondiffracting beams with computer-generated holograms," J. Opt. Soc. Am. A 6(11), 1748 (1989).
- 41. N. Chattrapiban, E. A. Rogers, D. Cofield, W. T. Hill, III, and R. Roy, "Generation of nondiffracting Bessel beams by use of a spatial light modulator," Opt. Lett. **28**(22), 2183 (2003).
- 42. C. Paterson and R. Smith, "Higher-order Bessel waves produced by axicon-type computer-generated holograms," Opt. Commun. **124**(1–2), 121–130 (1996).
- 43. X. Yu, A. Todi, and H. Tang, "Bessel beam generation using a segmented deformable mirror," Appl. Opt. 57(16), 4677 (2018).
- 44. H. Cheng, C. Xia, S. M. Kuebler, and X. Yu, "Aberration correction for SLM-generated Bessel beams propagating through tilted interfaces," Opt. Commun. **475**(June), 126213 (2020).
- 45. O. Mendoza-Yero, G. Mínguez-Vega, and J. Lancis, "Encoding complex fields by using a phase-only optical element," Opt. Lett. **39**(7), 1740 (2014).
- 46. L. B. Felsen and N. Marcuvitz, Radiation and Scattering of Waves (IEEE, 1994).
- 47. A. V. Osipov and S. A. Tretyakov, *Modern Electromagnetic Scattering Theory with Applications* (John Wiley & Sons, Ltd, 2017).
- 48. G. Whyte and J. Courtial, "Experimental demonstration of holographic three-dimensional light shaping using a Gerchberg–Saxton algorithm," New J. Phys. 7, 117–117 (2005).
- 49. P. Golvari and S. M. Kuebler, "Fabrication of Functional Microdevices in SU-8 by Multi-Photon Lithography," Micromachines **12**(5), 472 (2021).
- 50. S. Li, Z. Yang, J. Wang, and M. Zhao, "Broadband terahertz circular polarizers with single- and double-helical array metamaterials," J. Opt. Soc. Am. A **28**(1), 19 (2011).
- 51. Y. Yu, Z. Yang, M. Zhao, and P. Lu, "Broadband optical circular polarizers in the terahertz region using helical metamaterials," J. Opt. **13**(5), 055104 (2011).